Supplementary Information

Jiawei Chen [a, #], Runqing Zhang [b, #], Jiasheng Luo[a], Huafeng Dong[b,c,*], Jiachun Cao[d,*], Haojun Ling[b], Chuyu Li[b], Minru Wen[b] and Fugen Wu[e]

AFFILIATIONS

[a] School of Chemical Engineering and Light Industry, Guangdong University of Technology, Guangzhou 510006, China

[b] School of Physics and Optoelectronic Engineering, Guangdong University of Technology, Guangzhou 510006, China

[c] Guangdong provincial Key Laboratory of Information Photonics Technology, Guangdong University of Technology, Guangzhou 510006, China

[d] Institute of Environmental Health and Pollution Control, School of Environmental Science and Engineering, Guangdong University of Technology, Guangzhou, China

[e] School of Materials and Energy, Guangdong University of Technology, Guangzhou 510006, China

[#] Jiawei Chen and Runqing Zhang made equal contributions to this work

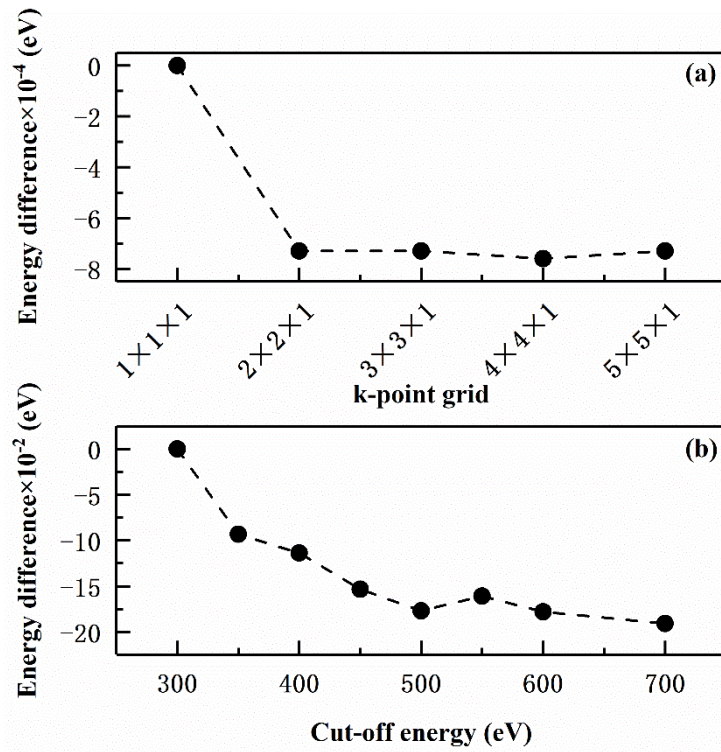[*] E-mail address: hfdong@gdut.edu.cn and caojiachun98@163.com.

Fig. S1 Convergence test for k-point grid and cut-off energy.

We performed convergence tests using V_S-HfS$_2$ as an example, and the results are shown in Fig. S1. The y-axis represents the energy differences compared to the first test (k-point of 1×1×1 and a plane wave cut-off energy of 300 eV).

As shown in Fig. S1(a), there is minimal energy variation between using a k-point of 2×2×1 and the one using a larger k-point, indicating that using a 3×3×1 k-point mesh in the SCF is reasonable.

Regarding the convergence test for the cut-off energy in Fig. S1(b), it was found that the energy converges when the cut-off energy larger than 450 eV, therefore the 500 eV we used meets the required precision for the calculations.

We calculated the defect formation energies (E_{df}) and formation energies (E_f) to investigate the stability of HfX$_2$ (X= S, Se, Te).
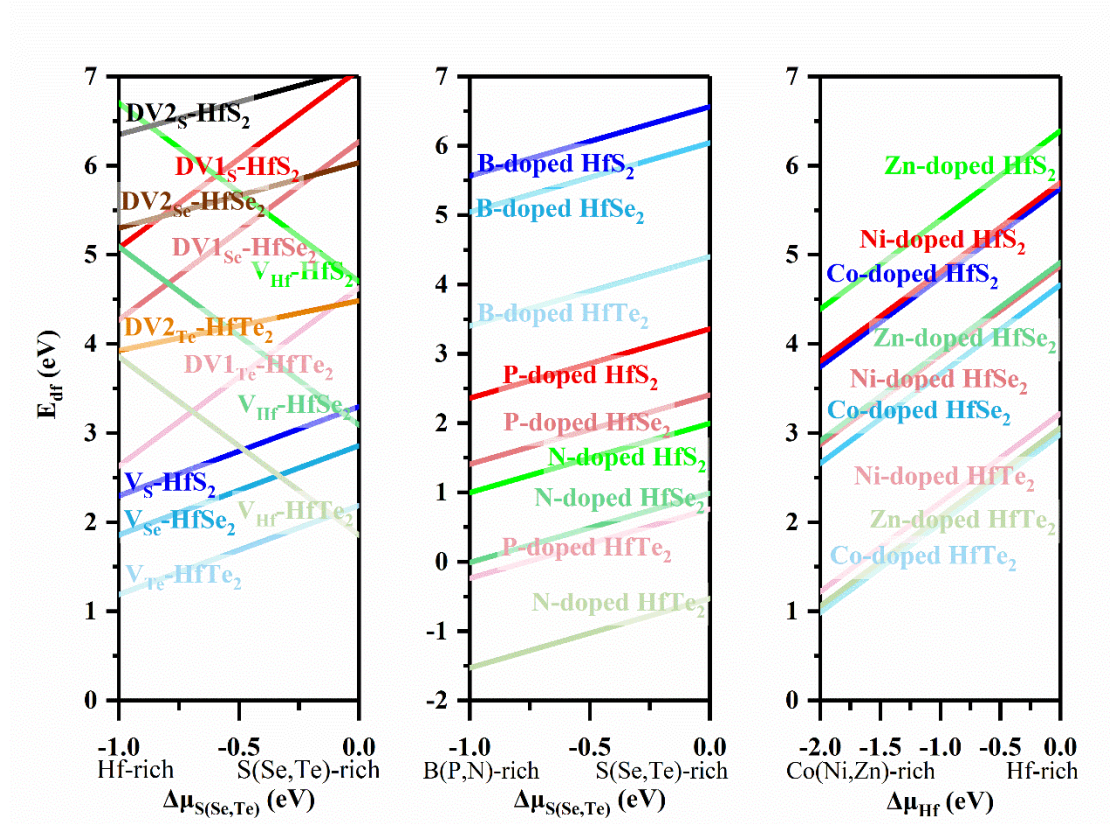

Fig. S2 The defect formation energies (E_{df}) of all defect structures.

The defect formation energy is calculated by the following equation:

$$E_{df} = E_D - E_P + \sum \Delta n_i \mu_i, \tag{1}$$

where E_D is the energy of defect structures and E_p is the energy of pristine structures, μ_i is the chemical potential of different atom species i, and Δn_i is the difference in atom species i between defective and pristine structures. Take Co-doped HfS$_2$ as an example, we consider Hf as a testing parameter. To maintain thermodynamic equilibrium ($\mu_{HfS2} = 16\mu_{Hf} + 32\mu_S$), the scope of μ_{Hf} is set to $\frac{E_{HfS2} - 32E_{S(bulk)}}{16} < \mu_{Hf} < E_{Hf(bulk)}$, where the upper limit corresponds to Hf-rich and the lower limit represents Co-rich(i.e., Hf-poor). In Fig. S2, it can be observed that the formation of most defects requires the absorption of heat.

Take Co-doped HfS_2 as an example, the E_f is calculated by the following equation:

$$E_f = \frac{E_{(Co-doped\ HfS2)} - (15\mu_{Hf} + \mu_{Co} + 32\mu_S)}{48}, \qquad (2)$$

where $E_{(Co-doped\ HfS2)}$ is the total energy of the monolayer Co-doped HfS_2 in the super cell, μ_{Hf}, μ_{Co}, and μ_S are the chemical potentials of Hf, Co, and S atoms, which were derived from the most stable phase, and "48" is the total number of atoms in the supercell. The formation energies of all structures shown in Table S1 are negative, indicating all the structures could exist at ambient pressure.
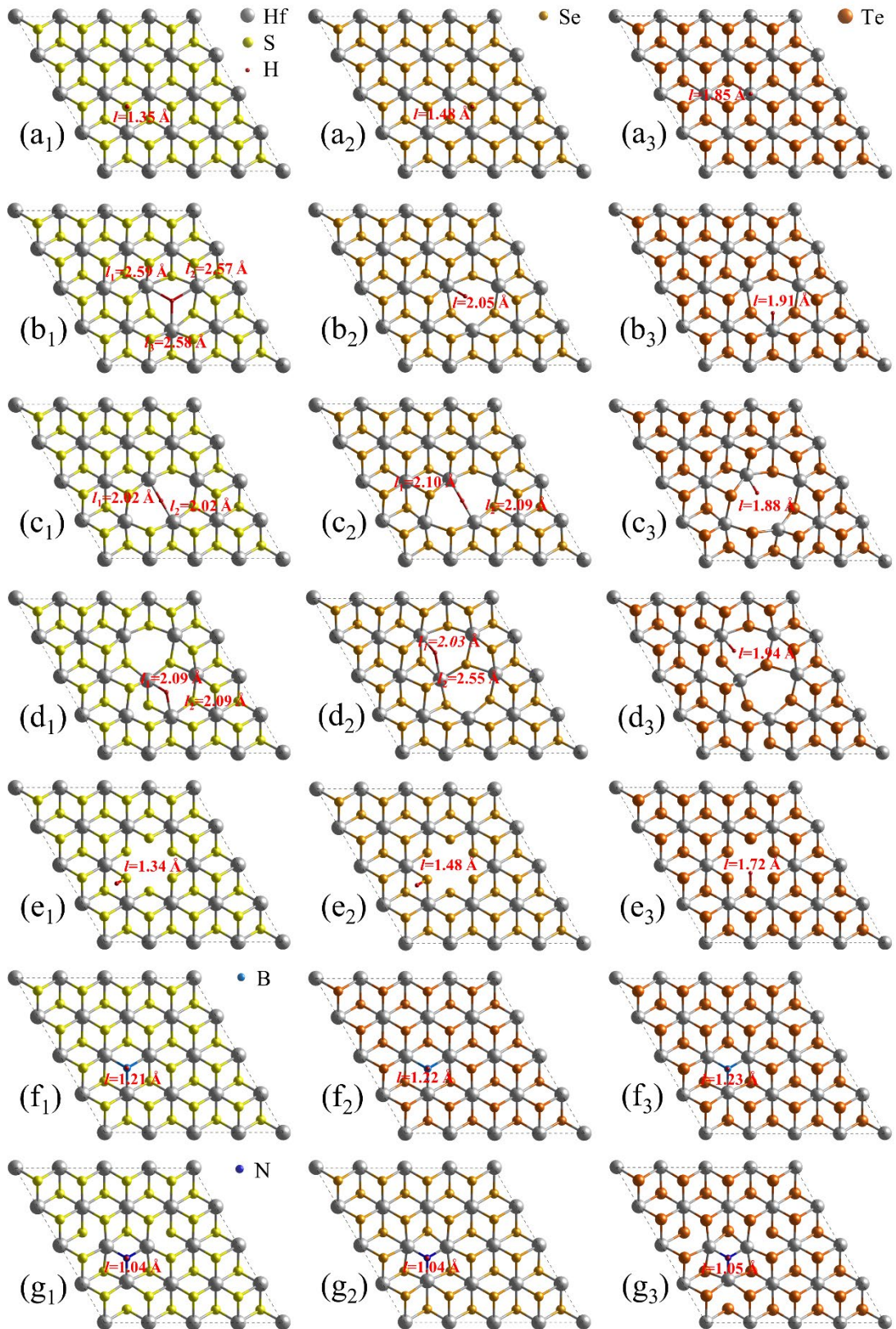
Table S1 The formation energy (eV) of defect structures.

The formation energy (eV)	HfS_2	$HfSe_2$	$HfTe_2$
Pristine	-1.59	-1.35	-0.81
$V_{S/Se/Te}$	-1.52	-1.29	-0.77
$DV1_{S/Se/Te}$	-1.47	-1.24	-0.73
$DV2_{S/Se/Te}$	-1.47	-1.25	-0.73
V_{Hf}	-1.39	-1.20	-0.72
B-doped	-1.37	-1.15	-0.66
Co-doped	-1.47	-1.25	-0.75
N-doped	-1.55	-1.33	-0.82
Ni-doped	-1.47	-1.25	-0.75
P-doped	-1.52	-1.30	-0.80
Zn-doped	-1.46	-1.25	-0.75

The corresponding content has been added to the Supplementary Information.

Table S2 The adsorption energy (eV) of H possible sites of pristine and defective structures shown in Fig. 1.

Defect type	Vacancy type /Doped atom	H-adsorption sites	HfS$_2$	HfSe$_2$	HfTe$_2$
pristine	/	site 1	1.10	1.32	1.25
		site 2	1.75	1.50	0.91
single vacancy of nonmetallic atom	V$_{S/Se/Te}$	site 1	0.22	2.29	0.45
		site 2	0.22	0.38	0.45
		site 3	0.22	1.33	1.27
		site 4	1.07	0.38	0.45
double vacancies of nonmetallic atom (type I)	DV1$_{S/Se/Te}$	site 1	-1.17	2.32	0.50
		site 2	-1.17	-0.03	1.02
		site 3	1.15	1.56	1.44
		site 4	-1.17	-0.03	0.22
		site 5	1.26	1.10	0.81
		site 6	-1.17	-1.16	-0.75
double vacancies of nonmetallic atom (type II)	DV2$_{S/Se/Te}$	site 1	-1.14	0.92	0.62
		site 2	1.90	2.07	1.78
		site 3	0.29	0.70	0.56
		site 4	0.22	0.84	1.55
		site 5	0.22	0.27	0.29
		site 6	0.21	0.24	1.11
single vacancy of metallic atom	V$_{Hf}$	site 1	-1.02	-0.43	0.06
		site 2	-1.02	-0.43	0.02
		site 3	-1.04	-0.44	0.04
		site 4	-1.04	-0.44	0.04
nonmetallic atom doping	B	site 1	-1.33	-1.16	-1.03
		site 2	1.53	1.21	0.94
		site 3	0.83	1.02	1.03
	N	site 1	-0.79	-0.08	0.70
		site 2	1.74	1.85	1.03
		site 3	0.05	0.81	1.30
	P	site 1	-0.96	-0.29	0.25
		site 2	-0.96	1.27	1.04
		site 3	0.19	0.86	1.29
metallic atom doping	Co	site 1	0.19	0.59	0.94
		site 2	-0.27	0.60	1.15
		site 3	1.29	1.37	1.10
	Ni	site 1	1.14	1.11	1.00
		site 2	0.26	0.66	0.94
		site 3	1.66	1.41	0.78
	Zn	site 1	0.69	0.87	1.09
		site 2	-0.47	0.19	0.69
		site 3	1.04	1.09	1.06

Legend:
- Hf
- S
- H
- Se
- Te
- B
- N

(a_1) $l=1.35$ Å
(a_2) $l=1.48$ Å
(a_3) $l=1.85$ Å

(b_1) $l_1=2.59$ Å, $l_2=2.57$ Å, $l_3=2.58$ Å
(b_2) $l=2.05$ Å
(b_3) $l=1.91$ Å

(c_1) $l_1=2.02$ Å, $l_2=2.02$ Å
(c_2) $l_1=2.10$ Å, $l_2=2.09$ Å
(c_3) $l=1.88$ Å

(d_1) $l_1=2.09$ Å, $l_2=2.09$ Å
(d_2) $l_1=2.03$ Å, $l_2=2.55$ Å
(d_3) $l=1.94$ Å

(e_1) $l=1.34$ Å
(e_2) $l=1.48$ Å
(e_3) $l=1.72$ Å

(f_1) $l=1.21$ Å
(f_2) $l=1.22$ Å
(f_3) $l=1.23$ Å

(g_1) $l=1.04$ Å
(g_2) $l=1.04$ Å
(g_3) $l=1.05$ Å
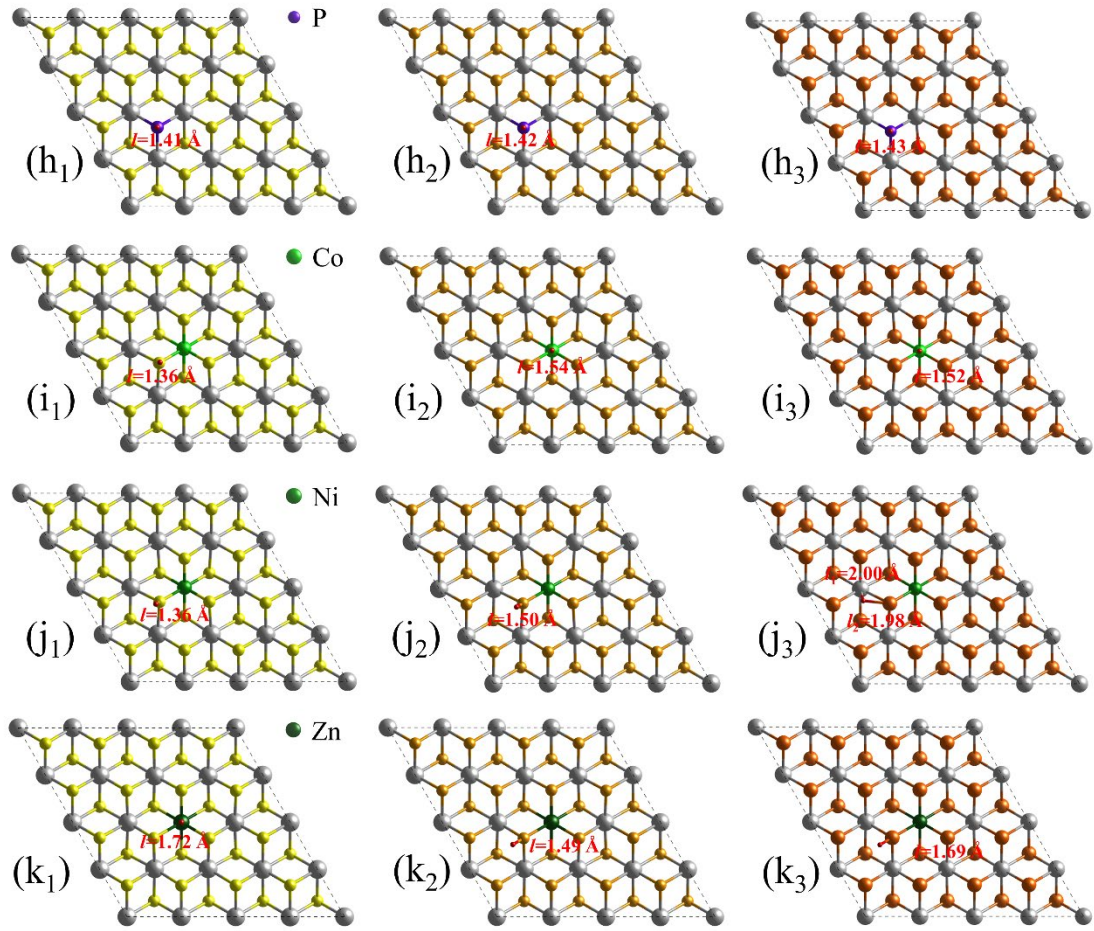
Fig. S3 The structures after optimized and the bond lengths(l) between H atom and catalyst.

In Fig. S3, (a) represent the structures of pristine, (b-e) represent the structures with single vacancy of nonmetallic atom, double vacancies of nonmetallic atom (type I), double vacancies of nonmetallic atom (type II) and single vacancy of metallic atom respectively, (f-k) represent the structures with B, N, P, Co, Ni or Zn atom doping respectively. The subscripts 1, 2, and 3 correspond to the host material is HfS_2, $HfSe_2$, and $HfTe_2$, respectively.
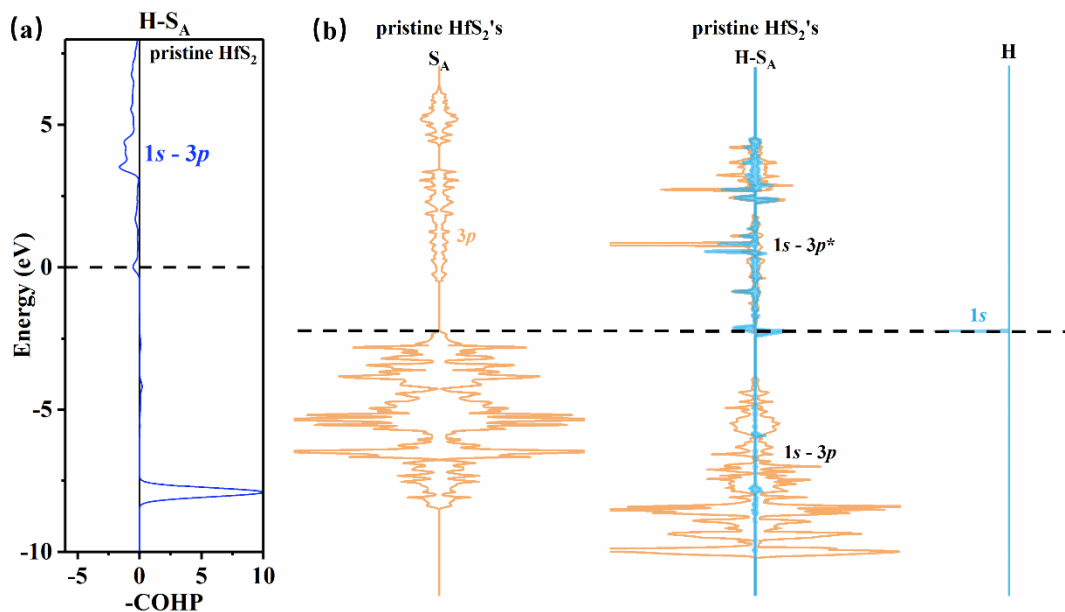
Fig. S4 The pCOHP (a) of H-S_A bonds of pristine HfS_2. The pDOS (b) of $3p$ orbitals of the S_A atom on pristine HfS_2, $1s$ orbital of H atom and their interaction.

In our analysis of Fig. 3(b), the interaction between the active site S atom (S_A atom) and the H atom will form the bonding and antibonding orbitals. For the pristine HfS_2's H-S_A bonds, the bonding orbital is completely filled with electrons, while the antibonding orbital is partially filled with electrons.

The projected crystal orbital Hamilton population (pCOHP) is to demonstrate the formation of bonding and antibonding orbitals (Fig. S4(a)). Additionally, we have plotted a comparison of the projected electronic density of states (pDOS) (Fig. S4(b)) to illustrate how the H atom interact with the monolayer.

The pCOHP of the H-S_A bonds is shown in Fig. S4(a). It is evident that a small part of the antibonding orbital of the $1s$ - $3p$ interaction is below the Fermi level, indicating partial occupation, thereby confirming our analysis: The 1s orbital of the H atom hybridizes with the $3p$ orbitals of the S_A atom, resulting in the formation of bonding and antibonding orbitals (Fig. S4(b)). The bonding orbital ($1s$ - $3p$) is completely filled with electrons, while the antibonding orbital ($1s$ - $3p*$) is partially filled with electrons.
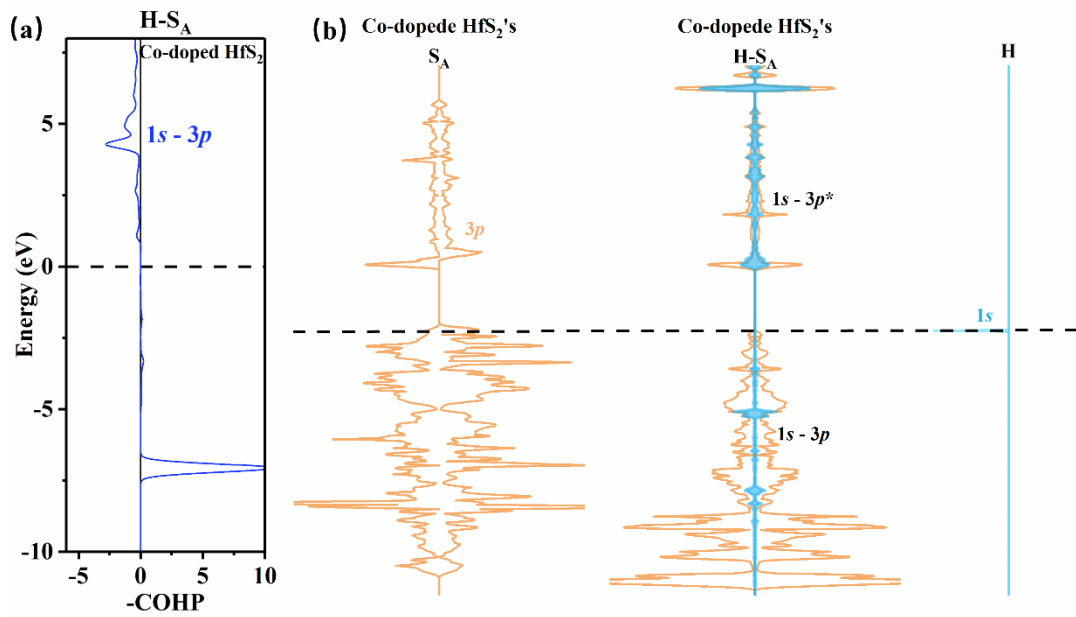
Fig. S5 The pCOHP (a) of H-S_A bonds of Co-doped HfS$_2$. The pDOS (b) of $3p$ orbitals of the S_A atom on Co-doped HfS$_2$, $1s$ orbital of H atom and their interaction.

In Fig. 3(b), the interaction between the S_A atom of Co-doped HfS$_2$ and the H atom form the bonding and antibonding orbitals. The bonding orbital is completely filled with electrons, while there is no electron filled in the antibonding orbital.

By observing the pCOHP of the H-S_A bonds in Fig. S5(a), the antibonding orbital of the $1s$ - $3p$ is completely situated above the Fermi level, with no electron filled with, and the bonding orbital is completely filled with electrons, confirming our inference: The $1s$ orbital of the H atom hybridizes with the $3p$ orbitals of the S_A atom, resulting in the formation of bonding and antibonding orbitals (Fig. S5(b)). The bonding orbital ($1s$ - $3p$) is completely filled with electrons, while there is no electron fill in the antibonding orbital ($1s$ - $3p^*$).
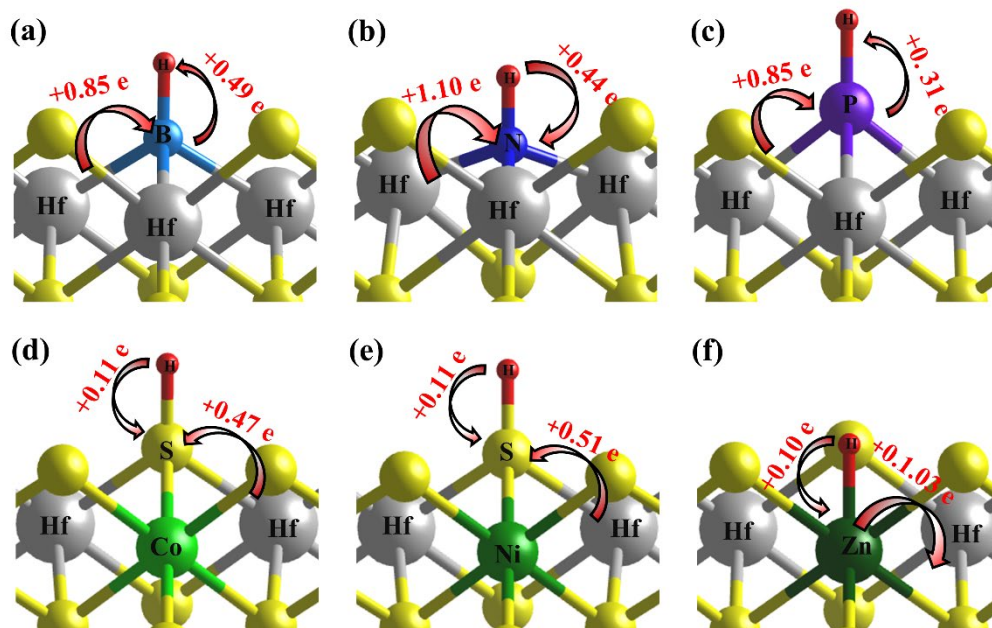
Fig. S6 The charge transfers of HfS$_2$ with B(a), N(b), P(c), Co(d), Ni(e), Zn(f) atom doping, respectively.
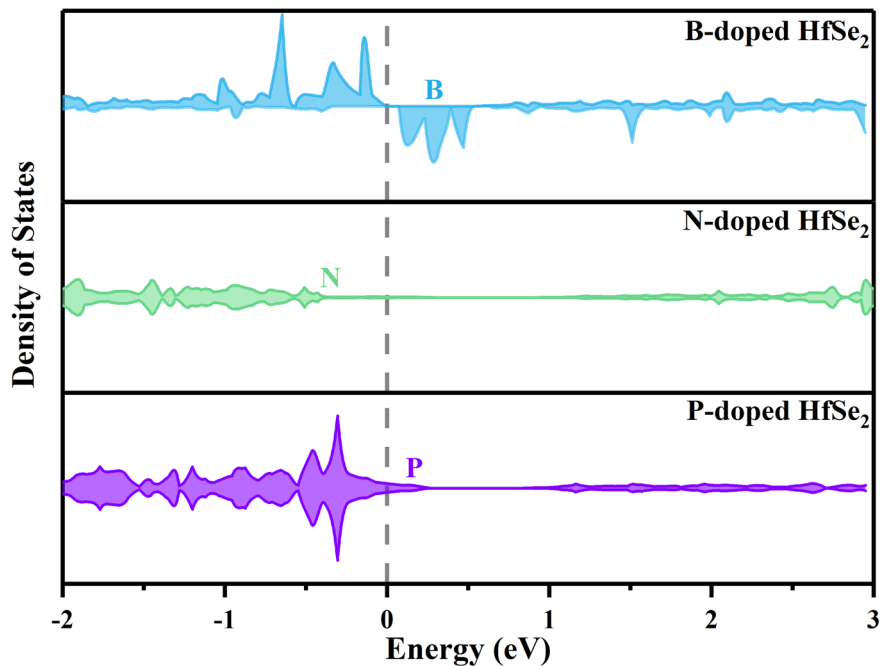
Fig. S7 The density of states of non-metallic atom-doped HfSe$_2$'s doping atom.

The greater the number of empty states near the fermi level (where the $1s$ state of H atom located), the stronger the interaction between H atom and those states[1]. We have conducted an analysis of non-metallic atom-doped HfSe$_2$'s electronic structure. As shown in Fig. S7, the introduction of B atoms induces a substantial number of defect states above the Fermi level, allowing for a strong interaction with H atom, which makes the desorption of generated hydrogen difficult ($\Delta E_H = -1.66$ eV, $\Delta G_H = -0.95$ eV). The N element doping scarcely generates defect states above the Fermi level and indicate N-doped HfSe$_2$ catalytic inertness ($\Delta E_H = -0.08$ eV, $\Delta G_H = 0.26$ eV). Concerning the P element doping, it induces a small amount of unoccupied states above the Fermi level, enabling it to form an appropriate strength of H-P bonds ($\Delta E_H = -0.29$ eV, $\Delta G_H = -0.02$ eV). Consequently, P-doped HfSe$_2$ is an excellent catalyst for hydrogen evolution.

REFERENCES

1.   An, Y.;   Fan, X.;   Liu, H.; Luo, Z., Improved catalytic performance of monolayer nano-triangles WS2 and MoS2 on HER by 3d metals doping. *Computational Materials Science* **2019,** *159*, 333-340.